

Dilepton rate and quark number susceptibility with the Gribov actionAritra Bandyopadhyay^{*}*Theory Division, Saha Institute of Nuclear Physics, 1/AF Bidhan Nagar, Kolkata 700064, India*Najmul Haque[†]*Physics Department, Kent State University, Kent, Ohio 44242, USA*Munshi G. Mustafa[‡]*Theory Division, Saha Institute of Nuclear Physics, 1/AF Bidhan Nagar, Kolkata 700064, India*Michael Strickland[§]*Physics Department, Kent State University, Kent, Ohio 44242, USA*

(Received 26 November 2015; published 2 March 2016)

We use a recently obtained resummed quark propagator at finite temperature which takes into account both the chromoelectric scale gT and the chromomagnetic scale g^2T through the Gribov action. The electric scale generates two massive modes whereas the magnetic scale produces a new massless spacelike mode in the medium. Moreover, the nonperturbative quark propagator is found to contain no discontinuity in contrast to the standard perturbative hard thermal loop approach. Using this nonperturbative quark propagator and vertices constructed using the Slavnov-Taylor identity, we compute the nonperturbative dilepton rate at vanishing three-momentum at one-loop order. The resulting rate has a rich structure at low energies due to the inclusion of the nonperturbative magnetic scale. We also calculate the quark number susceptibility, which is related to the conserved quark number density fluctuation in the deconfined state. Both the dilepton rate and quark number susceptibility are compared with results from lattice quantum chromodynamics and the standard hard thermal loop approach. Finally, we discuss how the absence of a discontinuity in the imaginary part of the nonperturbative quark propagator makes the results for both dilepton production and quark number susceptibility dramatically different from those in perturbative approaches and seemingly in conflict with known lattice data.

DOI: [10.1103/PhysRevD.93.065004](https://doi.org/10.1103/PhysRevD.93.065004)**I. INTRODUCTION**

The ongoing ultrarelativistic heavy-ion collision experiments at the RHIC and LHC enable us to study the quark-gluon plasma (QGP) which is a deconfined state of hadronic matter generated at very high temperatures and/or densities. Although the quark-gluon plasma may be strongly coupled at low temperatures, at high temperature there is evidence that resummed perturbation theory can be used to understand the properties of the QGP. To perturbatively study the QGP one needs to have an in-depth understanding of the various collective modes. These collective modes can be roughly classified into three types which are associated with different thermal scales, namely the energy (or hard) scale T , electric scale gT , and magnetic scale g^2T , where g is the strong coupling and T is the temperature of the system. The majority of studies in the literature have focused on the hard and electric scales, since the magnetic scale is related to the difficult nonperturbative physics of confinement.

Based on the hard-thermal-loop (HTL) resummations [1–3], a reorganization of finite-temperature perturbation theory called HTL perturbation theory (HTLpt) was developed over a decade ago [4]. HTLpt deals with the intrinsic energy scale T as the hard scale and the electric scale gT as the soft scale and has been extensively used to calculate various physical quantities associated with the deconfined state of matter. These quantities include the thermodynamic potential and other relevant quantities associated with it [4–23], photon production rate [24], dilepton production rate [25,26], single quark and quark-antiquark potentials [27,28], photon damping rate [29,30], fermion damping rate [31,32], gluon damping rate [2,33], plasma instabilities [34–36], jet energy loss [37–42], lepton asymmetry during leptogenesis [43,44], and thermal axion production [45].

Although HTLpt seems to work well at a temperature of approximately $2 T_c$ and above, where $T_c \sim 160$ MeV is the pseudocritical temperature for the QGP phase transition, the time-averaged temperature of the QGP generated at the RHIC and LHC energies is quite close to T_c . Near T_c , the running coupling g is large and the QGP could therefore be completely nonperturbative in this vicinity of the phase diagram. In order to make some progress at these

^{*} aritra.bandyopadhyay@saha.ac.in[†] nhaque@kent.edu[‡] munshigolam.mustafa@saha.ac.in[§] mstrick6@kent.edu

temperatures, it is necessary to consider the nonperturbative physics associated with the QCD magnetic scale in order to assess its role. Unfortunately, the magnetic scale is still a challenge for the theoreticians to treat in a systematic manner since, although its inclusion eliminates infrared divergences, the physics associated with the magnetic scale remains completely nonperturbative [46]. The fact that the $\mathcal{O}(g^2T)$ correction to the Debye mass receives nonperturbative contributions indicates that the background physics is fundamentally nonperturbative [47]. The physics in the magnetic sector is described by a dimensionally reduced three-dimensional Yang-Mills theory and the nonperturbative nature of the physics in this sector is related with the confining properties of the theory.

Lattice QCD (LQCD) provides a first-principles-based method that can take into account the nonperturbative effects of QCD. Lattice QCD has been used to probe the behavior of QCD in the vicinity of T_c , where matter undergoes a phase transition from the hadronic phase to the deconfined QGP phase. At this point, the QCD thermodynamic functions and some other relevant quantities associated with the fluctuations of conserved charges at finite temperature and zero chemical potential have been very reliably computed using LQCD (see e.g. Refs. [48–55]). In addition, quenched LQCD has also been used to study the structure of vector-meson correlation functions. Such studies have provided critically needed information about the thermal dilepton rate and various transport coefficients at zero momentum [56–59] and finite momentum [60].

Calculations in LQCD proceed by evaluating the Euclidean time correlation function only for a discrete and finite set of Euclidean times. To obtain the dilepton rate, one needs to perform an analytic continuation of the correlator from discrete Euclidean times to reconstruct the vector spectral function in continuous real time. However, this is an ill-posed problem. To proceed, the spectral function and hence the dilepton rate in continuous real time can be obtained from the correlator in discrete Euclidean times through a probabilistic interpretation based on the maximum entropy method (MEM) [61–63], which requires an ansatz for the spectral function. Employing a free-field spectral function as an ansatz, the spectral function in the quenched approximation of QCD was obtained earlier and found to approach zero in the low-energy limit [59]. In the same work, the authors found that the lattice dilepton rate approached zero at low invariant masses [59]. In a more recent LQCD calculation with larger lattice size, the authors used a Breit-Wigner (BW) form for low energies plus a free-field form for high energies as their ansatz for the spectral function [56]. The low-energy BW form of their ansatz gave a finite low-energy spectral function and low-mass dilepton rate. This indicates that the computation of a low-mass dilepton rate in LQCD is indeed a difficult task and it is also not very clear if there are

structures in the low-mass dilepton rate similar to those found in the HTLpt calculation [25].

Given the uncertainty associated with the lattice computation of dynamical quantities, e.g. spectral functions, the dilepton rate, and transport coefficients, it is desirable to have an alternative approach to include nonperturbative effects that can be handled in a similar way as in resummed perturbation theory. A few such approaches are available in the literature: one approach is a semi-empirical way to incorporate nonperturbative aspects by introducing a gluon condensate¹ in combination with the Green functions in momentum space, which has been proposed in e.g. Refs. [64–69]. In this approach, the effective n -point functions are related by Slavnov-Taylor (ST) identities which contain gluon condensates in the deconfined phase as hinted from lattice measurements in pure-gluon QCD [70]. The dispersion relations with dimension-four gluon condensates in medium exhibits two massive modes [64] (a normal quark mode and a plasmino mode) similar to HTL quark dispersion relations. This feature leads to sharp structures (van Hove singularities, an energy gap, etc.) in the dilepton production rates [66,71] at zero momentum, qualitatively similar to the HTLpt rate [25].

Using quenched LQCD, Refs. [72,73] calculated the Landau-gauge quark propagator and its corresponding spectral function by employing a two-pole ansatz corresponding to a normal quark and a plasmino mode following the HTL dispersion relations [25]. In a very recent approach [74], a Schwinger-Dyson equation has been constructed with the aforementioned Landau-gauge propagator obtained using quenched LQCD [72,73] and a vertex function related through the ST identity. Using this setup the authors computed the dilepton rate from the deconfined phase and found that it has the characteristic van Hove singularities but does not have an energy gap.

In a very recent approach [75] quark propagation in a deconfined medium including both electric- and magnetic-mass effects has also been studied by taking into account the nonperturbative magnetic screening scale by using the Gribov-Zwanziger (GZ) action [76,77], which regulates the magnetic IR behavior of QCD. Since the gluon propagator with the GZ action is IR regulated, this mimics confinement, making the calculations more compatible with results of LQCD and functional methods [78]. Interestingly, the resulting HTL-GZ quark collective modes consist of two massive modes (a normal quark mode and a plasmino mode) similar to the standard HTL dispersions along with a

¹An important aspect of the phase structure of QCD is to understand the effects of different condensates, which serve as order parameters of the broken symmetry phase. These condensates are nonperturbative in nature and their connection with bulk properties of QCD matter is provided by LQCD. The gluon condensate has a potentially substantial impact on the bulk properties, e.g., on the equation of state of QCD matter, compared to the quark condensate.

new massless spacelike excitation which is directly related to the incorporation of the magnetic scale through the GZ action. This new quark collective excitation results in a long-range correlation in the system, which may have important consequences for various physical quantities relevant for the study of deconfined QCD matter. In light of this, we would like to compute the dilepton production rate and the quark number susceptibility (QNS) associated with the conserved number fluctuation from the deconfined QGP using the nonperturbative GZ action.

This paper is organized as follows. In Sec. II we briefly outline the setup for quark propagation in a deconfined medium using the GZ action. In Sec. III we calculate the nonperturbative dilepton rate and discuss the results. Section IV describes the computation and results of non-perturbative QNS. In Sec. V we summarize and conclude.

II. SETUP

We know that gluons play an important role in confinement. In the GZ action [76,77] the issue of confinement is usually tackled kinematically with the gluon propagator in covariant gauge taking the form [76,77]

$$D^{\mu\nu}(P) = \left[\delta^{\mu\nu} - (1 - \xi) \frac{P^\mu P^\nu}{P^2} \right] \frac{P^2}{P^4 + \gamma_G^4}, \quad (1)$$

where the four-momenta $P = (p_0, \vec{p})$, ξ is the gauge parameter, and γ_G is called the *Gribov parameter*. The inclusion of the term involving γ_G in the denominator moves the poles of the gluon propagator off the energy axis so that there are no asymptotic gluon modes. Naturally, to maintain the consistency of the theory, these unphysical poles should not be considered in the exact correlation functions of gauge-invariant quantities. This suggests that the gluons are not physical excitations. In practice, this means that the inclusion of the Gribov parameter results in the effective confinement of gluons.

In QCD, the Gribov ambiguity typically results in multiple gauge-equivalent copies and, as a result, it renders perturbative QCD calculations ambiguous. However, the dimensionful Gribov parameter appearing above can acquire a well-defined meaning if the topological structure of the $SU(3)$ gauge group is made to be consistent with the theory. Very recently, this has been argued and demonstrated by Kharzeev and Levin [79] by taking into account the periodicity of the θ vacuum [80] of the theory due to the compactness of the $SU(3)$ gauge group. The recent work of Kharzeev and Levin indicates that the Gribov term can be physically interpreted as the topological susceptibility of pure Yang-Mills theory and that confinement is built into the gluon propagator in Eq. (1), indicating nonpropagation of color charges at long distances and screening of color charges at long distances in the running coupling. This also reconciles the original view Zwanziger had regarding γ_G being a statistical parameter [77]. In practice, γ_G can be

self-consistently determined using a one-loop gap equation and at asymptotically high temperatures it takes the following form [75,81,82]:

$$\gamma_G = \frac{D-1}{D} \frac{N_c}{4\sqrt{2}\pi} g^2 T, \quad (2)$$

where D is the dimension of the theory and N_c is the number of colors.² The one-loop running strong coupling, $g^2 = 4\pi\alpha_s$, is

$$g^2(T) = \frac{48\pi^2}{(33 - 2N_f) \ln\left(\frac{Q_0^2}{\Lambda_0^2}\right)}, \quad (3)$$

where N_f is the number of quark flavors and Q_0 is the renormalization scale, which is usually chosen to be $2\pi T$ unless specified. We fix the scale Λ_0 by requiring that $\alpha_s(1.5 \text{ GeV}) = 0.326$, as obtained from lattice measurements [84]. For one-loop running, this procedure gives $\Lambda_0 = 176 \text{ MeV}$.

To study the properties of a hot QGP using (semi) perturbative methods, the effective quark propagator is an essential ingredient. After resummation, the quark propagator can be expressed as

$$iS^{-1}(P) = \not{P} - \Sigma(P), \quad (4)$$

where $\Sigma(P)$ is the quark self-energy. One can calculate Σ using the modified gluon propagator (1) in the high-temperature limit to obtain [75]

$$\begin{aligned} \Sigma(P) &= (ig)^2 C_F \not{\mathcal{F}}_{\{K\}} \gamma_\mu S_f(K) \gamma_\nu D^{\mu\nu}(P-K) \\ &\approx -(ig)^2 C_F \sum_{\pm} \int_0^\infty \frac{dk}{2\pi^2} k^2 \int \frac{d\Omega}{4\pi} \\ &\quad \times \frac{\tilde{n}_{\pm}(k, \gamma_G)}{4E_{\pm}^0} \left[\frac{i\gamma_0 + \hat{\mathbf{k}} \cdot \boldsymbol{\gamma}}{iP_0 + k - E_{\pm}^0 + \frac{\mathbf{p} \cdot \mathbf{k}}{E_{\pm}^0}} \right. \\ &\quad \left. + \frac{i\gamma_0 - \hat{\mathbf{k}} \cdot \boldsymbol{\gamma}}{iP_0 - k + E_{\pm}^0 - \frac{\mathbf{p} \cdot \mathbf{k}}{E_{\pm}^0}} \right], \end{aligned} \quad (5)$$

where $\not{\mathcal{F}}_{\{K\}}$ is a fermionic sum-integral, $S_f(K)$ is the bare quark propagator, and

$$\begin{aligned} \tilde{n}_{\pm}(k, \gamma_G) &\equiv n_B\left(\sqrt{k^2 \pm i\gamma_G^2}\right) + n_F(k), \\ E_{\pm}^0 &= \sqrt{k^2 \pm i\gamma_G^2}, \end{aligned} \quad (6)$$

where n_B and n_F are Bose-Einstein and Fermi-Dirac distribution functions, respectively. The modified thermal

²Equation (2) is a one-loop result. In the vacuum, the two-loop result has been determined [83] and the Gribov propagator form (1) is unmodified. Only γ_G itself is modified to take into account the two-loop correction. To the best of our knowledge, this would hold also at finite temperature.

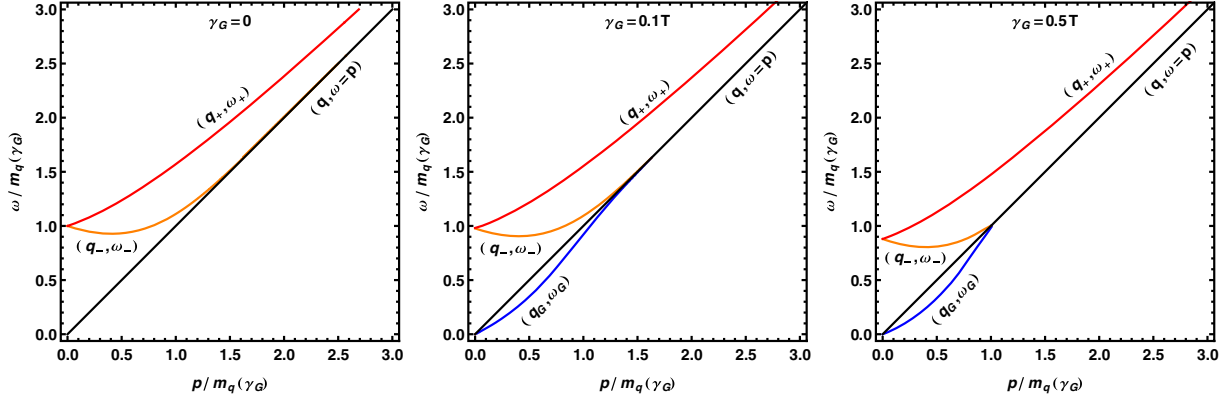


FIG. 1. Plot of the dispersion relations for different values of γ_G . In the parentheses, the first one represents a collective excitation mode whereas the second one is the corresponding energy of that mode.

quark mass in the presence of the Gribov term can also be obtained as

$$m_q^2(\gamma_G) = \frac{g^2 C_F}{4\pi^2} \sum_{\pm} \int_0^{\infty} dk \frac{k^2}{E_{\pm}^0} \tilde{n}_{\pm}(k, \gamma_G). \quad (7)$$

Using the modified quark self-energy given in Eq. (5), it is now easy to write down the modified effective quark propagator in the presence of the Gribov term as

$$iS^{-1}(P) = A_0 \gamma_0 - A_s \gamma \cdot \hat{\mathbf{p}}, \quad (8)$$

where, keeping the structure typically used within the HTL approximation, A_0 and A_s are defined as [75]

$$\begin{aligned} A_0(\omega, p) &= \omega - \frac{2g^2 C_F}{(2\pi)^2} \sum_{\pm} \int dkk \tilde{n}_{\pm}(k, \gamma_G) [Q_0(\tilde{\omega}_1^{\pm}, p) + Q_0(\tilde{\omega}_2^{\pm}, p)], \\ A_s(\omega, p) &= p + \frac{2g^2 C_F}{(2\pi)^2} \sum_{\pm} \int dkk \tilde{n}_{\pm}(k, \gamma_G) [Q_1(\tilde{\omega}_1^{\pm}, p) + Q_1(\tilde{\omega}_2^{\pm}, p)]. \end{aligned} \quad (9)$$

Here the modified frequencies are defined as $\tilde{\omega}_1^{\pm} \equiv E_{\pm}^0(\omega + k - E_{\pm}^0)/k$ and $\tilde{\omega}_2^{\pm} \equiv E_{\pm}^0(\omega - k + E_{\pm}^0)/k$. The Legendre functions of the second kind, Q_0 and Q_1 , are

$$Q_0(\omega, p) \equiv \frac{1}{2p} \ln \frac{\omega + p}{\omega - p}, \quad (10)$$

$$Q_1(\omega, p) \equiv \frac{1}{p} (1 - \omega Q_0(\omega, p)). \quad (11)$$

Using the helicity representation, the modified effective fermion propagator can also be written as

$$iS(P) = \frac{1}{2} \frac{(\gamma_0 - \gamma \cdot \hat{\mathbf{p}})}{D_+} + \frac{1}{2} \frac{(\gamma_0 + \gamma \cdot \hat{\mathbf{p}})}{D_-}, \quad (12)$$

where D_{\pm} are obtained as

$$\begin{aligned} D_+(\omega, p, \gamma_G) &= A_0(\omega, p) - A_s(\omega, p) \\ &= \omega - p - \frac{2g^2 C_F}{(2\pi)^2} \sum_{\pm} \int dkk \tilde{n}_{\pm}(k, \gamma_G) \\ &\quad \times [Q_0(\tilde{\omega}_1^{\pm}, p) + Q_1(\tilde{\omega}_1^{\pm}, p) \\ &\quad + Q_0(\tilde{\omega}_2^{\pm}, p) + Q_1(\tilde{\omega}_2^{\pm}, p)], \\ D_-(\omega, p, \gamma_G) &= A_0(\omega, p) + A_s(\omega, p) \\ &= \omega + p - \frac{2g^2 C_F}{(2\pi)^2} \sum_{\pm} \int dkk \tilde{n}_{\pm}(k, \gamma_G) \\ &\quad \times [Q_0(\tilde{\omega}_1^{\pm}, p) - Q_1(\tilde{\omega}_1^{\pm}, p) \\ &\quad + Q_0(\tilde{\omega}_2^{\pm}, p) - Q_1(\tilde{\omega}_2^{\pm}, p)]. \end{aligned} \quad (13)$$

Solving for the zeros of $D_{\pm}^{-1}(P, \gamma_G)$ gives the dispersion relations for the collective excitations in the medium. In Fig. 1 we show the resulting dispersion relations for three different values of the Gribov parameter γ_G . In the absence of the Gribov term (i.e., $\gamma_G = 0$), there are two massive modes corresponding to a normal quark mode q_+ with energy ω_+ and a long-wavelength plasmino mode q_- with energy ω_- that quickly approaches free massless propagation in the high-momentum limit. These two modes are similar to those found in the HTL approximation [25]. With the inclusion of the Gribov term, there is a massless mode q_G with energy ω_G , in addition to the two massive modes, q_+ and q_- [75]. The extra mode q_G is due to the presence of the magnetic screening scale. This new massless mode is lightlike at large momenta.³ In this context, we note that in Ref. [69], such an extra massive mode with a significant

³The slope of the dispersion relation for this extra massless spacelike mode q_G exceeds unity in some domain of momentum. Thus, the group velocity, $d\omega_G/dp$, is superluminal for the spacelike mode q_G and approaches the light cone ($d\omega/dp = 1$) from above at high momentum. Since the mode is spacelike, there is no causality problem. Instead, this represents anomalous dispersion in the presence of the GZ action which converts Landau damping into amplification of the spacelike dispersive mode.

spectral width was observed near T_c in the presence of dimension-four gluon condensates [69] in addition to the usual propagating quark and plasmino modes. The existence of this extra mode could affect lattice extractions of the dilepton rate since even the most recent LQCD results [72,73] assumed that there were only two poles (a quark mode and a plasmino mode) inspired by the HTL approximation.

In the HTL approximation ($\gamma_G = 0$) the propagator contains a discontinuity in the complex plane stemming from the logarithmic terms in Eq. (13) due to spacelike momentum $\omega^2 < p^2$. Apart from two collective excitations originating from the in-medium dispersion as discussed above, there is also a Landau cut contribution in the spectral representation of the propagator due to the discontinuity in spacelike momentum. On the other hand, for $\gamma_G \neq 0$ the individual terms in Eq. (13) possess discontinuities at spacelike momentum but are canceled out when all terms are summed owing to the fact that the poles come in complex-conjugate pairs. As a result, there is no discontinuity in the complex plane.⁴ This results in the disappearance of the Landau cut contribution in the spectral representation of the propagator in the spacelike domain. It appears as if the Landau cut contribution in the spacelike domain for $\gamma_G = 0$ is replaced by a massless spacelike dispersive mode in the presence of the magnetic scale ($\gamma_G \neq 0$). So the spectral function corresponding to the propagator D_{\pm}^{-1} for $\gamma_G \neq 0$ has only pole contributions. As a result, one has

$$\rho_{\pm}^G(\omega, p) = \frac{\omega^2 - p^2}{2m_q^2(\gamma_G)} [\delta(\omega \mp \omega_+) + \delta(\omega \pm \omega_-) + \delta(\omega \pm \omega_G)], \quad (14)$$

where D_+ has poles at ω_+ , $-\omega_-$, and $-\omega_G$ and D_- has poles at ω_- , $-\omega_+$, and ω_G with a prefactor, $(\omega^2 - p^2)/2m_q^2(\gamma_G)$, as the residue.

At this point we would like to mention that the non-perturbative quark spectral function obtained using the quark propagator analyzed in the quenched LQCD calculations of Refs. [72–74] and utilizing gluon condensates in Refs. [64–66,69,71] also forbids a Landau cut contribution since the effective quark propagators in these calculations do not contain any discontinuities. This stems from the fact that the quark self-energies in Refs. [64–66,69,71] do not have any imaginary parts whereas in Refs. [72–74] an ansatz of two quasiparticles was employed for the spectral function based on the LQCD quark propagator analyzed in the quenched approximation. The spectral function

⁴Starting from the Euclidean expression (5), we have numerically checked for discontinuities and found none. We found some cusp-like structures at complex momenta, but Σ was found to be C^0 continuous everywhere in the complex plane.

obtained with the Gribov action (14) also possesses only pole contributions but no Landau cut. As a result, this approach completely removes the quasiglons responsible for the Landau cut that should be present in a high-temperature quark-gluon plasma. This is similar to findings in other nonperturbative approaches [64–66,71–74]. We will return to the consequences of the absence of the Landau cut in the results and conclusions sections.

Returning to the problem at hand, the spectral density in Eq. (14) at vanishing three-momentum ($p \equiv |\vec{p}| = 0$) contains three delta function singularities corresponding to the two massive modes and one new massless Gribov mode. To proceed, one needs the vertex functions in the presence of the Gribov term. These can be determined by explicitly computing the hard-loop limit of the vertex function using the Gribov propagator. One can verify, after the fact, that the resulting effective quark-gluon vertex function satisfies the necessary ST identity

$$(P_1 - P_2)_\mu \Gamma^\mu(P_1, P_2) = S^{-1}(P_1) - S^{-1}(P_2). \quad (15)$$

The temporal and spatial parts of the modified effective quark-gluon vertex can be written as

$$\begin{aligned} \Gamma^0 &= a_G \gamma^0 + b_G \boldsymbol{\gamma} \cdot \hat{\mathbf{p}}, \\ \Gamma^i &= c_G \gamma^i + b_G \hat{p}^i \gamma_0 + d_G \hat{p}^i (\boldsymbol{\gamma} \cdot \hat{\mathbf{p}}), \end{aligned} \quad (16)$$

where the coefficients are given by

$$\begin{aligned} a_G &= 1 - \frac{2g^2 C_F}{(2\pi)^2} \sum_{\pm} \int dkk \tilde{n}_{\pm}(k, \gamma_G) \frac{1}{\omega_1 - \omega_2} [\delta Q_{01}^{\pm} + \delta Q_{02}^{\pm}], \\ b_G &= -\frac{2g^2 C_F}{(2\pi)^2} \sum_{\pm} \int dkk \tilde{n}_{\pm}(k, \gamma_G) \frac{1}{\omega_1 - \omega_2} [\delta Q_{11}^{\pm} + \delta Q_{12}^{\pm}], \\ c_G &= 1 + \frac{2g^2 C_F}{(2\pi)^2} \sum_{\pm} \int dkk \tilde{n}_{\pm}(k, \gamma_G) \\ &\quad \times \frac{1}{3(\omega_1 - \omega_2)} [\delta Q_{01}^{\pm} + \delta Q_{02}^{\pm} - \delta Q_{21}^{\pm} - \delta Q_{22}^{\pm}], \\ d_G &= \frac{2g^2 C_F}{(2\pi)^2} \sum_{\pm} \int dkk \tilde{n}_{\pm}(k, \gamma_G) \frac{1}{\omega_1 - \omega_2} [\delta Q_{21}^{\pm} + \delta Q_{22}^{\pm}], \end{aligned}$$

with

$$\begin{aligned} \delta Q_{n1}^{\pm} &= Q_n(\tilde{\omega}_{11}^{\pm}, p) - Q_n(\tilde{\omega}_{21}^{\pm}, p) \quad \text{for } n = 0, 1, 2, \\ \omega_{m1}^{\pm} &= E_{\pm}^0(\omega_m + k - E_{\pm}^0)/k \quad \text{for } m = 1, 2, \\ \omega_{m2}^{\pm} &= E_{\pm}^0(\omega_m - k + E_{\pm}^0)/k \quad \text{for } m = 1, 2. \end{aligned}$$

Similarly, the four-point function can be obtained by computing the necessary diagrams in the hard-loop limit and it satisfies the following generalized ST identity:

$$\begin{aligned} P_\mu \Gamma^{\mu\nu}(-P_1, P_1; -P_2, P_2) &= \Gamma^\nu(P_1 - P_2, -P_1; P_2) \\ &\quad - \Gamma^\nu(-P_1 - P_2, P_1; P_2). \end{aligned} \quad (17)$$

III. ONE-LOOP DILEPTON PRODUCTION WITH THE GRIBOV ACTION

The dilepton production rate for a dilepton with energy ω and three-momentum \vec{q} is related to the discontinuity of the photon self-energy $\Pi^{\mu\nu}(Q)$ as [85]

$$\frac{dR}{d\omega d^3q} = \frac{\alpha}{12\pi^3 Q^2} \frac{1}{e^{\beta\omega} - 1} \frac{1}{2\pi i} \text{Disc}\Pi_\mu^\mu(Q). \quad (18)$$

At one-loop order, the dilepton production rate is related to the two diagrams shown in Fig. 2, which can be written as

$$\Pi_\mu^\mu(Q) = \frac{5}{3} e^2 \sum_{p_0} \int \frac{d^3p}{(2\pi)^3} \{ \text{Tr}[S(P)\Gamma_\mu(K, Q, -P)S(K)\Gamma_\mu(-K, -Q, P)] + \text{Tr}[S(P)\Gamma_\mu^\mu(-P, P; -Q, Q)] \}, \quad (19)$$

where $K = P - Q$. The second term in Eq. (19) is due to the tadpole diagram shown in Fig. 2 which, in the end, does not contribute since $\Gamma_\mu^\mu = 0$. However, the tadpole diagram is essential to satisfy the transversality condition, $Q_\mu \Pi^{\mu\nu}(Q) = 0$ and thus gauge invariance and charge conservation in the system.

Using the n -point functions computed in Sec. II and performing traces, one obtains

$$\begin{aligned} \Pi_\mu^\mu(\vec{q} = 0) = & \frac{10}{3} e^2 T \sum_{p_0} \int \frac{d^3p}{(2\pi)^3} \left[\left\{ \frac{(a_G + b_G)^2}{D_+(\omega_1, p, \gamma_G) D_-(\omega_2, p, \gamma_G)} + \frac{(a_G - b_G)^2}{D_-(\omega_1, p, \gamma_G) D_+(\omega_2, p, \gamma_G)} \right\} \right. \\ & - \left\{ \frac{(c_G + b_G + d_G)^2}{D_+(\omega_1, p, \gamma_G) D_-(\omega_2, p, \gamma_G)} + \frac{(c_G - b_G + d_G)^2}{D_-(\omega_1, p, \gamma_G) D_+(\omega_2, p, \gamma_G)} \right\} \\ & \left. - 2c_G^2 \left\{ \frac{1}{D_+(\omega_1, p, \gamma_G) D_+(\omega_2, p, \gamma_G)} + \frac{1}{D_-(\omega_1, p, \gamma_G) D_-(\omega_2, p, \gamma_G)} \right\} \right]. \quad (20) \end{aligned}$$

The discontinuity can be obtained by the Braaten-Pisarski-Yuan (BPY) prescription [25]

$$\text{Disc} T \sum_{p_0} f_1(p_0) f_2(q_0 - p_0) = 2\pi i (1 - e^{\beta\omega}) \int d\omega_1 \int d\omega_2 n_F(\omega_1) n_F(\omega_2) \delta(\omega - \omega_1 - \omega_2) \rho_1(\omega_1) \rho_2(\omega_2), \quad (21)$$

which, after some work, allows one to determine the dilepton rate at zero three-momentum

$$\begin{aligned} \frac{dR}{d\omega d^3q}(\vec{q} = 0) = & \frac{10\alpha^2}{9\pi^4} \frac{1}{\omega^2} \int_0^\infty p^2 dp \int_{-\infty}^\infty d\omega_1 \int_{-\infty}^\infty d\omega_2 n_F(\omega_1) n_F(\omega_2) \delta(\omega - \omega_1 - \omega_2) \\ & \times \left[4 \left(1 - \frac{\omega_1^2 - \omega_2^2}{2p\omega} \right)^2 \rho_+^G(\omega_1, p) \rho_-^G(\omega_2, p) \right. \\ & + \left(1 + \frac{\omega_1^2 + \omega_2^2 - 2p^2 - 2m_q^2(\gamma_G)}{2p\omega} \right)^2 \rho_+^G(\omega_1, p) \rho_+^G(\omega_2, p) \\ & \left. + \left(1 - \frac{\omega_1^2 + \omega_2^2 - 2p^2 - 2m_q^2(\gamma_G)}{2p\omega} \right)^2 \rho_-^G(\omega_1, p) \rho_-^G(\omega_2, p) \right]. \quad (22) \end{aligned}$$

Using Eq. (14) and considering all physically allowed processes by the in-medium dispersion, the total contribution can be expressed as

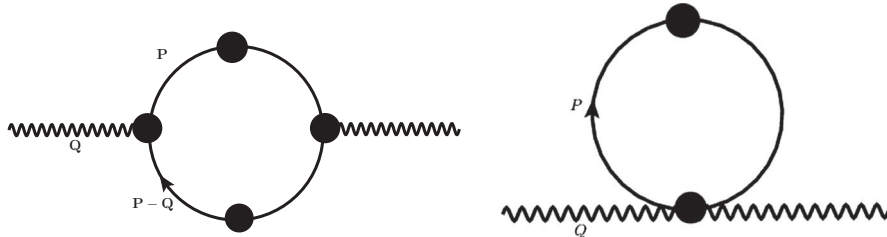


FIG. 2. The self-energy (left) and tadpole (right) diagrams at one-loop order.

$$\begin{aligned}
\left. \frac{dR}{d\omega d^3q} \right|^{pp} (\vec{q} = 0) &= \frac{10\alpha^2}{9\pi^4} \frac{1}{\omega^2} \int_0^\infty p^2 dp \\
&\times \left[\delta(\omega - 2\omega_+) n_F^2(\omega_+) \left(\frac{\omega_+^2 - p^2}{2m_q^2(\gamma_G)} \right)^2 \left\{ 1 + \frac{\omega_+^2 - p^2 - m_q^2(\gamma_G)}{p\omega} \right\}^2 \right. \\
&+ \delta(\omega - 2\omega_-) n_F^2(\omega_-) \left(\frac{\omega_-^2 - p^2}{2m_q^2(\gamma_G)} \right)^2 \left\{ 1 - \frac{\omega_-^2 - p^2 - m_q^2(\gamma_G)}{p\omega} \right\}^2 \\
&+ \delta(\omega - 2\omega_G) n_F^2(\omega_G) \left(\frac{\omega_G^2 - p^2}{2m_q^2(\gamma_G)} \right)^2 \left\{ 1 - \frac{\omega_G^2 - p^2 - m_q^2(\gamma_G)}{p\omega} \right\}^2 \\
&+ 4\delta(\omega - \omega_+ - \omega_-) n_F(\omega_+) n_F(\omega_-) \left(\frac{\omega_+^2 - p^2}{2m_q^2(\gamma_G)} \right) \left(\frac{\omega_-^2 - p^2}{2m_q^2(\gamma_G)} \right) \\
&\times \left\{ 1 - \frac{\omega_+^2 - \omega_-^2}{2p\omega} \right\}^2 \\
&+ \delta(\omega - \omega_+ + \omega_-) n_F(\omega_+) n_F(-\omega_-) \left(\frac{\omega_+^2 - p^2}{2m_q^2(\gamma_G)} \right) \left(\frac{\omega_-^2 - p^2}{2m_q^2(\gamma_G)} \right) \\
&\times \left. \left\{ 1 + \frac{\omega_+^2 + \omega_-^2 - 2p^2 - 2m_q^2(\gamma_G)}{2p\omega} \right\}^2 \right]. \tag{23}
\end{aligned}$$

By inspecting the arguments of the various energy-conserving δ functions in Eq. (23) one can understand the physical processes originating from the poles of the propagator. The first three terms in Eq. (23) correspond to the annihilation processes of $q_+ \bar{q}_+ \rightarrow \gamma^*$, $q_- \bar{q}_- \rightarrow \gamma^*$, and $q_G \bar{q}_G \rightarrow \gamma^*$, respectively. The fourth term corresponds to the annihilation of $q_+ \bar{q}_- \rightarrow \gamma^*$. On the other hand, the fifth term corresponds to a process, $q_+ \rightarrow q_- \gamma^*$, where a q_+ mode makes a transition to a q_- mode along with a virtual

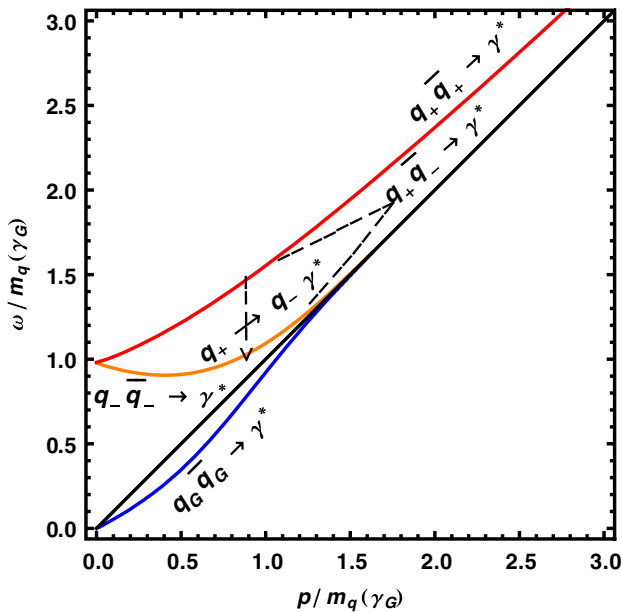


FIG. 3. Various dilepton processes which originate from the in-medium dispersion with the Gribov term.

photon. These processes involve soft quark modes (q_+ , q_- , and q_G and their antiparticles) which originate by cutting the self-energy diagram in Fig. 2 through the internal lines without a “blob.” The virtual photon, γ^* , in all these five processes decays to a lepton pair and can be visualized from the dispersion plot as displayed in Fig. 3. The momentum integration in Eq. (23) can be performed using the standard delta function identity

$$\delta(f(x)) = \sum_i \frac{\delta(x - x_i)}{|f'(x)|_{x=x_i}}, \tag{24}$$

where x_i are the solutions of $f(x_i) = 0$.

The contribution of various individual processes to the dilepton production rate in the presence of the Gribov term are displayed in the Fig. 4. Note that in this figure and in subsequent figures showing the dilepton rate, the vertical axis shows the dimensional late dilepton rate $dR/d^4p = dN/d^4x d^4p$ and the horizontal axis is scaled by the thermal quark mass as to make it dimensionless. In Fig. 4 we see that the transition process, $q_+ \rightarrow q_- \gamma^*$, begins at the energy $\omega = 0$ and ends up with a van Hove peak⁵ where all of the transitions from the q_+ branch are directed towards the minimum of the q_- branch. The annihilation process involving the massless spacelike Gribov modes, $q_G \bar{q}_G \rightarrow \gamma^*$, also starts at $\omega = 0$ and falls off very quickly. The annihilation of the two plasmino modes, $q_- \bar{q}_- \rightarrow \gamma^*$, opens up with again a van Hove peak at $\omega = 2 \times$ the minimum energy of the plasmino mode. The contribution

⁵A van Hove peak [86,87] appears where the density of states diverges as $f'(x)|_{x=x_0} = 0$ since the density of states is inversely proportional to $f'(x)$.

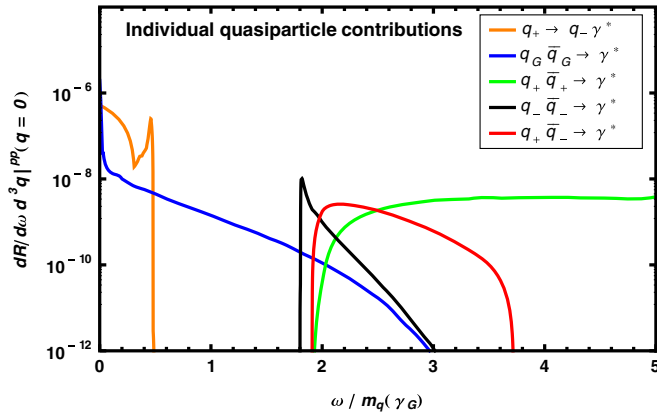


FIG. 4. The dilepton production rates corresponding to quasiparticle processes in Fig. 3.

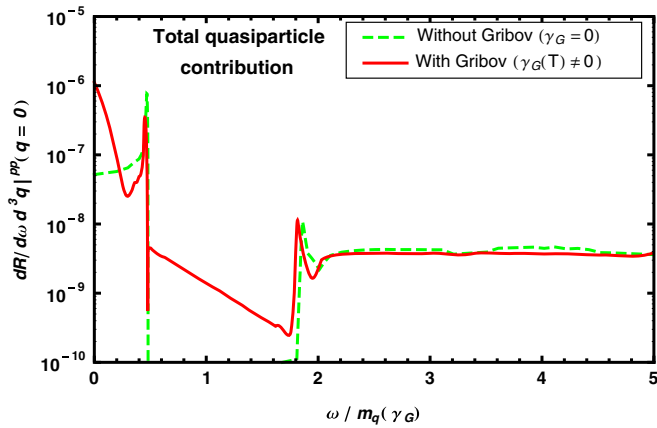


FIG. 5. Comparison of dilepton production rates involving various quasiparticle modes with and without the inclusion of γ_G .

of this process decreases exponentially. At $\omega = 2m_q(\gamma_G)$, the annihilation processes involving usual quark modes, $q_+\bar{q}_+ \rightarrow \gamma^*$, and that of a quark and a plasmino mode, $q_+\bar{q}_- \rightarrow \gamma^*$, begin. However, the former one ($q_+\bar{q}_+ \rightarrow \gamma^*$) grows with the energy and would converge to the usual Born rate (leading-order perturbative rate) [88] at high mass whereas the latter one ($q_+\bar{q}_- \rightarrow \gamma^*$) initially grows at a very fast rate, but then decreases slowly and finally drops very quickly. The behavior of the latter process can easily be understood from the dispersion properties of the quark and plasmino mode. Summing up, the total contribution of all these five processes is displayed in Fig. 5. This is compared with the similar dispersive contribution when $\gamma_G = 0$ [25], comprising the processes $q_+ \rightarrow q_- \gamma^*$, $q_+\bar{q}_+ \rightarrow \gamma^*$, $q_-\bar{q}_- \rightarrow \gamma^*$ and $q_+\bar{q}_- \rightarrow \gamma^*$. We note that when $\gamma_G = 0$, the dilepton rate contains both van Hove peaks and an energy gap [25]. In the presence of the Gribov term ($\gamma_G \neq 0$), the van Hove peaks remain, but the energy gap disappears due to the annihilation of new massless Gribov modes, $q_G \bar{q}_G \rightarrow \gamma^*$.

In Fig. 6 we compare the rates obtained using various approximations: the leading-order perturbative (Born) rate

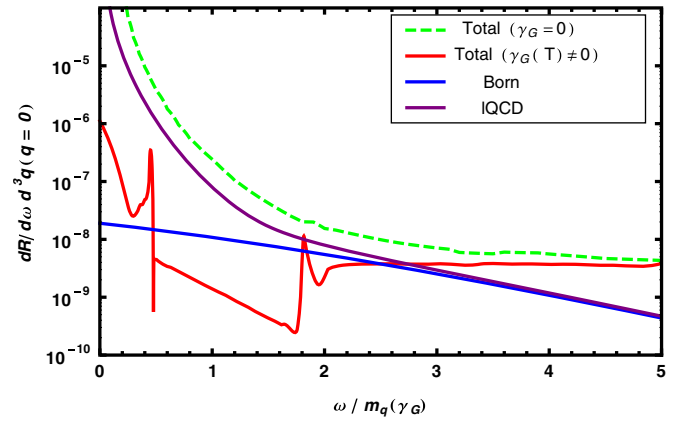


FIG. 6. Comparison of various dilepton production rates from the deconfined matter.

[88], the quenched LQCD rate [56,59], and with and without the Gribov term. The nonperturbative rate with the Gribov term shows important structures compared to the Born rate at low energies. But when compared to the total HTLpt rate⁶ it is suppressed in the low-mass region due to the absence of the Landau cut contribution for $\gamma_G \neq 0$. It seems as if the higher-order Landau cut contribution due to spacelike momenta for $\gamma_G = 0$ is replaced by the soft process involving spacelike Gribov modes in the collective excitations for $\gamma_G \neq 0$. We also note that the dilepton rate [74] using the spectral function constructed with the two-pole ansatz by analyzing the LQCD propagator in the quenched approximation [72,73] shows a similar structure as that found here for $\gamma_G \neq 0$. On the other hand, such a structure at low mass is also expected in the direct computation of the dilepton rate from LQCD in the quenched approximation [56,59]. However, a smooth variation of the rate was found at low mass. The computation of the dilepton rate in LQCD involves various intricacies and uncertainties. This is because, as noted in Sec. I, the spectral function in continuous time is obtained from the correlator in the finite set of discrete Euclidean time using a probabilistic MEM method [61–63] with a somewhat *ad hoc* continuous ansatz for the spectral function at low energy and also fundamental difficulties in performing the necessary analytic continuation in LQCD. Until LQCD overcomes the uncertainties and difficulties in the computation of the vector spectral function, one needs to depend, at this juncture, on the prediction of the effective approaches for the dilepton rate at low mass in particular. We further note that at high energies the rate for both $\gamma_G = 0$ and $\gamma_G \neq 0$ is higher than the lattice data and Born rate. This is a consequence of using the HTL self-energy also at high energies/

⁶Since the HTL spectral function (i.e., $\gamma_G = 0$) has both a pole and a Landau cut contribution, the HTLpt rate [25] contains an additional higher-order contribution due to the Landau cut stemming from spacelike momenta.

momentum where the soft-scale approximation breaks down. Nevertheless, the low mass rate obtained here by employing the nonperturbative magnetic scale ($\gamma_G \neq 0$) in addition to the electric scale allows for a model-based inclusion of the effect of confinement and the result has a somewhat rich structure at low energy compared to that obtained using only the electric scale ($\gamma_G = 0$) as well in LQCD.

We make some general comments concerning the dilepton rate below. If one looks at the dispersion plots in Fig. 1 for $\gamma_G = 0$, one finds that ω_- falls off exponentially and approaches the light cone, whereas ω_+ does not fall off exponentially to the light cone, but instead behaves as $[p + m_q^2(T)/p]$ for large p . On the other hand, in the presence of $\gamma_G \neq 0$ both ω_- and ω_G approach the light cone very quickly, but again ω_+ has a similar asymptotic behavior as before. This feature of ω_+ makes the dilepton rate at large ω in Fig. 6 saturated for both $\gamma_G = 0$ and $\gamma_G \neq 0$, because the dominant contribution comes from the annihilation of two ω_+ 's as discussed in Fig. 4. In general, the total dilepton rate in Fig. 6, behaves as $\sim \exp(-\omega/T)$ for $\gamma_G(T) = 0$ due to the Landau damping contribution coming from the quasiguons in a hot and dense medium. As the Landau cut contribution is missing in the $\gamma_G(T) \neq 0$ case, one finds a leveling off at low ω . In other words, since the Landau damping contribution is absent for $\gamma_G(T) \neq 0$, the rate approaches that of the pole-pole contribution for $\gamma_G = 0$ as shown in Fig. 5, except in the mass gap region. We further note that the LQCD rate [56] matches the Born rate at large ω simply because a free spectral function has been assumed for large ω . On the other hand the LQCD spectral function [56] at low ω is sensitive to the prior assumptions and, in such a case, the spectral function extracted using MEM [61–63] analyses should be interpreted carefully with a proper error analysis [61]. Since the MEM analyses are sensitive to the prior assumption, but are not very sensitive to the structure of the spectral function at small ω , the error is expected to be significant at

small ω . The existence of fine structures such as van Hove singularities at small ω cannot be excluded based on the LQCD rate [56] at this moment in time.

IV. ONE-LOOP QUARK NUMBER SUSCEPTIBILITY WITH THE GRIBOV ACTION

We now turn to the computation of the QNS including the Gribov term. The QNS can be interpreted as the response of the conserved quark number density, n with infinitesimal variation in the quark chemical potentials $\mu + \delta\mu$. In QCD thermodynamics it is defined as the second-order derivative of the pressure \mathcal{P} with respect to the quark chemical potential, μ . But again, using the fluctuation-dissipation theorem, the QNS for a given quark flavor can also be defined from the time-time component of the current-current correlator in the vector channel [6,8,89,90]. The QNS is in general expressed as

$$\begin{aligned} \chi_q(T) &= \left. \frac{\partial n}{\partial \mu} \right|_{\mu \rightarrow 0} = \left. \frac{\partial^2 \mathcal{P}}{\partial^2 \mu} \right|_{\mu \rightarrow 0} = \int d^4x \langle J_0(0, \vec{x}) J_0(0, \vec{0}) \rangle \\ &= \beta \int_{-\infty}^{\infty} \frac{d\omega}{2\pi} \frac{-2}{1 - e^{-\beta\omega}} \text{Im} \Pi_{00}(\omega, \vec{0}), \end{aligned} \quad (25)$$

where J_0 is the temporal component of the vector current and Π_{00} is the time-time component of the vector correlator or self-energy with external four-momenta $Q \equiv (\omega, \vec{q})$. The above relation in Eq. (25) is known as the thermodynamic sum rule [89,90] where the thermodynamic derivative with respect to the external source, μ is related to the time-time component of the static correlation function in the vector channel.

In order to compute the QNS we need to calculate the imaginary part of the temporal component of the two one-loop diagrams given in Fig. 2. The contribution of the self-energy diagram is

$$\Pi_{00}^s(Q) = N_f N_c T \sum_{p_0} \int \frac{d^3 p}{(2\pi)^3} \text{Tr}[S(P) \Gamma^0(K, Q, -P) S(K) \Gamma^0(-K, -Q, P)], \quad (26)$$

where $K = P - Q$. After performing the traces of the self-energy diagram, one obtains

$$\Pi_{00}^s(\vec{q} = 0) = 2N_f N_c T \sum_{p_0} \int \frac{d^3 p}{(2\pi)^3} \left[\frac{(a_G + b_G)^2}{D_+(\omega_1, p, \gamma_G) D_-(\omega_2, p, \gamma_G)} + \frac{(a_G - b_G)^2}{D_-(\omega_1, p, \gamma_G) D_+(\omega_2, p, \gamma_G)} \right], \quad (27)$$

where

$$\begin{aligned} a_G + b_G &= 1 - \frac{2g^2 C_F}{(2\pi)^2} \sum_{\pm} \int dk k \tilde{n}_{\pm}(k, \gamma_G) \frac{1}{\omega} [Q_0(\tilde{\omega}_{11}^{\pm}, p) + Q_1(\tilde{\omega}_{11}^{\pm}, p) + Q_0(\tilde{\omega}_{21}^{\pm}, p) - Q_1(\tilde{\omega}_{21}^{\pm}, p) \\ &\quad + Q_0(\tilde{\omega}_{12}^{\pm}, p) + Q_1(\tilde{\omega}_{12}^{\pm}, p) + Q_0(\tilde{\omega}_{22}^{\pm}, p) - Q_1(\tilde{\omega}_{22}^{\pm}, p)] \\ &= 1 + \frac{1}{\omega} [D_+(\omega_1, p, \gamma_G) + D_-(\omega_2, p, \gamma_G) - \omega_1 - \omega_2] \\ &= 1 - \frac{\omega_1 + \omega_2}{\omega} + \frac{D_+(\omega_1, p, \gamma_G) + D_-(\omega_2, p, \gamma_G)}{\omega}, \end{aligned} \quad (28)$$

and

$$\begin{aligned}
a_G - b_G &= 1 - \frac{2g^2 c_F}{(2\pi)^2} \sum_{\pm} \int dk k \tilde{n}_{\pm}(k, \gamma_G) \frac{1}{\omega} [Q_0(\tilde{\omega}_{11}^{\pm}, p) - Q_1(\tilde{\omega}_{11}^{\pm}, p) + Q_0(\tilde{\omega}_{21}^{\pm}, p) + Q_1(\tilde{\omega}_{21}^{\pm}, p) \\
&\quad + Q_0(\tilde{\omega}_{12}^{\pm}, p) - Q_1(\tilde{\omega}_{12}^{\pm}, p) + Q_0(\tilde{\omega}_{22}^{\pm}, p) + Q_1(\tilde{\omega}_{22}^{\pm}, p)] \\
&= 1 + \frac{1}{\omega} [D_-(\omega_1, p, \gamma_G) + D_+(\omega_2, p, \gamma_G) - \omega_1 - \omega_2] \\
&= 1 - \frac{\omega_1 + \omega_2}{\omega} + \frac{D_-(\omega_1, p, \gamma_G) + D_+(\omega_2, p, \gamma_G)}{\omega}, \tag{29}
\end{aligned}$$

where $D_{\mp}(\omega, p, \gamma_G)$ were defined in Eq. (13). We write only those terms of Eq. (27) which contain discontinuities

$$\begin{aligned}
\frac{(a_G + b_G)^2}{D_+(\omega_1, p, \gamma_G)D_-(\omega_2, p, \gamma_G)} &= \frac{(1 - \frac{\omega_1 + \omega_2}{\omega})^2}{D_+(\omega_1, p, \gamma_G)D_-(\omega_2, p, \gamma_G)} + \frac{1}{\omega^2} \left\{ \frac{D_+(\omega_1, p, \gamma_G)}{D_-(\omega_2, p, \gamma_G)} + \frac{D_-(\omega_2, p, \gamma_G)}{D_+(\omega_1, p, \gamma_G)} \right\}, \\
\frac{(a_G - b_G)^2}{D_-(\omega_1, p, \gamma_G)D_+(\omega_2, p, \gamma_G)} &= \frac{(1 - \frac{\omega_1 + \omega_2}{\omega})^2}{D_-(\omega_1, p, \gamma_G)D_+(\omega_2, p, \gamma_G)} + \frac{1}{\omega^2} \left\{ \frac{D_-(\omega_1, p, \gamma_G)}{D_+(\omega_2, p, \gamma_G)} + \frac{D_+(\omega_2, p, \gamma_G)}{D_-(\omega_1, p, \gamma_G)} \right\}. \tag{30}
\end{aligned}$$

Calculating the discontinuity using the BPY prescription given in Eq. (21), one can write the imaginary part of Eq. (27) as

$$\begin{aligned}
\text{Im}\Pi_{00}^s &= 4N_c N_f \pi (1 - e^{\beta\omega}) \int \frac{d^3 p}{(2\pi)^3} \int d\omega_1 \int d\omega_2 \delta(\omega - \omega_1 - \omega_2) n_F(\omega_1) n_F(\omega_2) \\
&\quad \times \left[\left(1 - \frac{\omega_1 + \omega_2}{\omega}\right)^2 \rho_+^G(\omega_1, p) \rho_-^G(\omega_2, p) + \frac{C_1 \rho_+^G(\omega_2, p) + C_2 \rho_-^G(\omega_2, p)}{\omega^2} \right], \tag{31}
\end{aligned}$$

with

$$\begin{aligned}
C_1 &= \text{Im}D_-(\omega_1, p) = 0, \\
C_2 &= \text{Im}D_+(\omega_1, p) = 0. \tag{32}
\end{aligned}$$

The tadpole part of Fig. 2 can now be written as

$$\Pi_{00}^t(Q) = N_f N_c T \sum_{p_0} \int \frac{d^3 p}{(2\pi)^3} \text{Tr}[S(P)\Gamma_{00}(-P, P; -Q, Q)]. \tag{33}$$

The four-point function Γ_{00} at zero three-momentum can be obtained using Eq. (17) giving

$$\begin{aligned}
\Gamma^{00} &= -(e_G \gamma^0 + f_G \hat{p} \cdot \vec{\gamma}), \\
e_G &= \frac{2g^2 c_F}{(2\pi)^2} \sum_{\pm} \int dk k \tilde{n}_{\pm}(k, \gamma_G) \frac{1}{(\omega_1 - \omega_2)} [\delta Q_{01}^{\pm} + \delta Q_{02}^{\pm} + \delta Q_{01}^{\pm'} + \delta Q_{02}^{\pm'}], \\
f_G &= \frac{2g^2 c_F}{(2\pi)^2} \sum_{\pm} \int dk k \tilde{n}_{\pm}(k, \gamma_G) \frac{1}{(\omega_1 - \omega_2)} [\delta Q_{11}^{\pm} + \delta Q_{12}^{\pm} + \delta Q_{11}^{\pm'} + \delta Q_{12}^{\pm'}], \tag{34}
\end{aligned}$$

where

$$\begin{aligned}
\delta Q_{n1}^{\pm'} &= Q_n(\tilde{\omega}_{11}^{\pm}, p) - Q_n(\tilde{\omega}_{21}^{\pm'}, p) \quad \text{for } n = 0, 1, 2, \\
\tilde{\omega}_{21}^{\pm'} &= E_{\pm}^0(\omega'_2 + k - E_{\pm}^0)/k, \\
\tilde{\omega}_{22}^{\pm'} &= E_{\pm}^0(\omega'_2 - k + E_{\pm}^0)/k, \\
\omega'_2 &= \omega_1 + \omega.
\end{aligned}$$

Proceeding in a similar way as in the self-energy diagram, the contribution from the tadpole diagram is

$$\begin{aligned} \text{Im}\Pi'_{00} &= -4N_c N_f \pi (1 - e^{\beta\omega}) \int \frac{d^3 p}{(2\pi)^3} \int d\omega_1 \int d\omega_2 \delta(\omega - \omega_1 - \omega_2) \frac{n_F(\omega_1) n_F(\omega_2)}{\omega^2} \\ &\times [C_1 \rho_+^G(\omega_2, p) + C_2 \rho_-^G(\omega_2, p)] = 0. \end{aligned} \quad (35)$$

The total imaginary contribution of the temporal part shown in Fig. 2 can now be written as

$$\begin{aligned} \text{Im}\Pi_{00} &= \text{Im}\Pi_{00}^s + \text{Im}\Pi'_{00} \\ &= 4N_c N_f \pi (1 - e^{\beta\omega}) \int \frac{d^3 p}{(2\pi)^3} \int d\omega_1 \int d\omega_2 \delta(\omega - \omega_1 - \omega_2) n_F(\omega_1) n_F(\omega_2) \left[\left(1 - \frac{\omega_1 + \omega_2}{\omega}\right)^2 \rho_+^G(\omega_1, p) \rho_-^G(\omega_2, p) \right]. \end{aligned} \quad (36)$$

It is clear from Eqs. (31) and (35) that the tadpole contribution in Eq. (35) exactly cancels with the second term of Eq. (31) even if C_1 and C_2 are finite, e.g., for the HTL case ($\gamma_G = 0$) [6,8]. At finite γ_G , the form of the sum of self-energy and tadpole diagrams remains the same, even though the individual contributions are modified.

Putting this in the expression for the QNS in Eq. (25), we obtain

$$\begin{aligned} \chi_q(T) &= 4N_c N_f \beta \int \frac{d^3 p}{(2\pi)^3} \int_{-\infty}^{\infty} d\omega \int d\omega_1 \int d\omega_2 \delta(\omega - \omega_1 - \omega_2) n_F(\omega_1) n_F(\omega_2) \left[\left(1 - \frac{\omega_1 + \omega_2}{\omega}\right)^2 \rho_+^G(\omega_1, p) \rho_-^G(\omega_2, p) \right] \\ &= 4N_c N_f \beta \int \frac{d^3 p}{(2\pi)^3} \left[\left(\frac{\omega_+^2 - p^2}{2m_q^2(\gamma_G)}\right)^2 n_F(\omega_+) n_F(-\omega_+) \right. \\ &\quad \left. + \left(\frac{\omega_-^2 - p^2}{2m_q^2(\gamma_G)}\right)^2 n_F(\omega_-) n_F(-\omega_-) + \left(\frac{\omega_G^2 - p^2}{2m_q^2(\gamma_G)}\right)^2 n_F(\omega_G) n_F(-\omega_G) \right] \\ &= \chi_q^{\text{pp}}(T) \end{aligned} \quad (37)$$

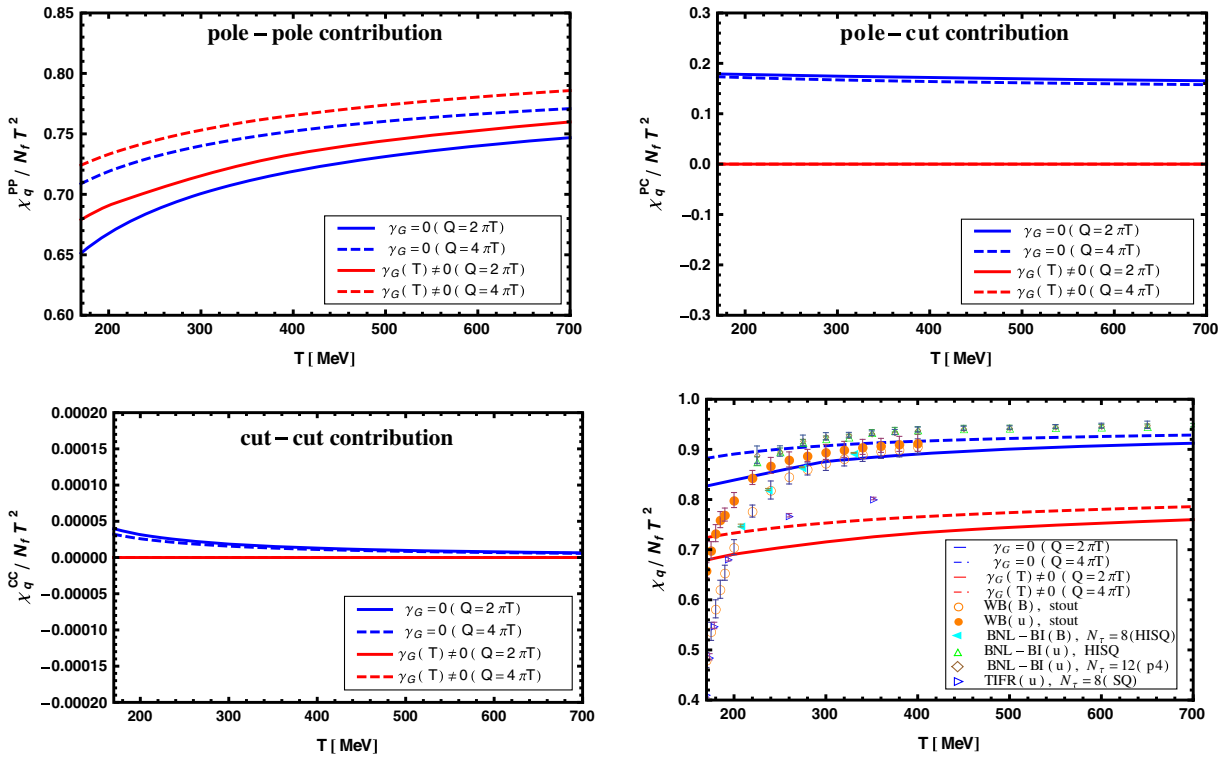


FIG. 7. The QNS scaled with free values is compared with and without the inclusion of γ_G . In each case a band appears due to the choice of the two renormalization scales as $2\pi T$ and $4\pi T$. The various symbols correspond to LQCD data from various groups labeled as WB [48], BNL-BI(B) and BNL-BI(u) [50,51], and TIFR [55].

where we represent the total $\chi_q(T)$ as $\chi_q^{\text{pp}}(T)$ since there is only the pole-pole contribution for $\gamma_G \neq 0$. However for $\gamma_G = 0$ there will be pole-cut [$\chi_q^{\text{pc}}(T)$] and cut-cut [$\chi_q^{\text{cc}}(T)$] contributions in addition to the pole-pole contribution because the spectral function contains the pole part + Landau cut contribution of the quark propagator.

In Fig. 7 we present the different contributions of the QNS scaled with the corresponding free values with and without the Gribov term. We, at first, note that the running coupling in Eq. (3) is a smooth function of T around and below T_c . We have extended to low temperatures as an extrapolation of our high-temperature result even though our treatment is strictly not valid below T_c . Now from the first panel of Fig. 7, the pole-pole contribution to the QNS with the Gribov action is increased at low T , compared to that in the absence of the Gribov term. This improvement at low T is solely due to the presence of the nonperturbative Gribov mode in the collective excitations. However, at high T both contributions become almost the same as the Gribov mode disappears. There are no pole-cut (pc) or cut-cut (cc) contributions for $\gamma_G(T) \neq 0$, compared to that for $\gamma_G = 0$. The pc and cc contributions in the absence of the magnetic scale are displayed in the second and third panels. As a result, we find that the QNS in the presence of the magnetic scale contains only the pp contribution due to collective excitations originating from the in-medium dispersion whereas, in the absence of the magnetic scale, the QNS is enhanced due to an additional higher-order Landau cut (i.e., pole-cut + cut-cut) contribution as shown in the fourth panel. When compared with LQCD data from various groups [48,50,51,55], the QNS in the presence of the magnetic scale lies around (10–15)% below the LQCD results whereas that in the absence of the magnetic scale is very close to LQCD data. This is expected due to the *additional higher-order Landau cut* contribution in the absence of the magnetic scale as discussed earlier. This also suggests that it is necessary to include higher-loop orders in the QNS in the presence of the magnetic scale, which is beyond the scope of this paper. However, we hope to carry out this nontrivial task in the near future.

V. CONCLUSIONS AND OUTLOOK

In this paper we considered the effect of the inclusion of magnetic screening in the context of the Gribov-Zwanziger picture of confinement. In covariant gauge, this was accomplished by adding a mass-like parameter, the Gribov parameter, to the bare gluon propagator resulting in the nonpropagation of gluonic modes. Following Ref. [75] we obtained the resummed quark propagator taking into account the Gribov parameter. A new key feature of the resulting resummed quark propagator is that it contains no discontinuities. In the standard perturbative hard-thermal-loop approach there are discontinuities at

spacelike momentum associated with Landau damping which seem to be absent in the GZ-HTL approach. Using the resulting quark propagator, we evaluated the spectral function, finding that it only contains poles for $\gamma_G \neq 0$. We then used these results to compute (1) the dilepton production rate at vanishing three-momentum and (2) the quark number susceptibility. For the dilepton production rate, we found that, due to the absence of Landau damping for $\gamma_G \neq 0$, the rate contains sharp structures, e.g. van Hove singularities, which do not seem to be present in the lattice data. That being said, since the lattice calculations used a perturbative ansatz for the spectral function when performing their MEM analysis [61] of the spectral function, it is unclear how changing the underlying prior assumptions about the spectral function would affect the final lattice results. Moreover, the error analysis for the spectral function with the MEM prescription [62] has to be done more carefully than it was done in the LQCD calculation [56]. Since the result is sensitive to the prior assumptions, the error seems to become large and as a result no conclusion can be drawn for fine structures at low mass dileptons from the LQCD result. For the quark number susceptibilities, we found that, again due to the absence of Landau damping for $\gamma_G \neq 0$, the results do not agree well with available lattice data. This can be contrasted with a standard HTLpt calculation, which seems to describe the lattice data quite well with no free parameters. It is possible that higher-order loop calculations could improve the agreement between the Gribov-scenario results and the lattice data; however, the success of HTLpt compared to lattice data as well as nonperturbative model calculations suggests that at $T \gtrsim 200$ MeV the electric sector alone provides an accurate description of QGP thermodynamics. Nevertheless, the present HTLpt results pose a serious challenge to the Gribov scenario for only the inclusion of magnetic mass effects in the QGP. The absence of quasi-gluons responsible for the Landau cut makes the results for both dilepton production and the quark number susceptibility dramatically different from those in perturbative approaches. We conclude that the results with the present GZ action are in conflict with those in perturbative approaches due to the absence of the Landau cut contribution in the nonperturbative quark propagator.

ACKNOWLEDGMENTS

We would like to thank N. Su, K. Tywoniuk, W. Florkowski, and P. Petreczky for useful conversations. A.B. and M.G.M. were supported by the Indian Department of Atomic Energy. N.H. was supported by the Indian Department of Atomic Energy and an award from the Kent State University Office of Research and Sponsored Programs. M.S. was supported by the U.S. Department of Energy under Award No. DE-SC0013470.

- [1] E. Braaten and R. D. Pisarski, Soft amplitudes in hot gauge theories: A general analysis, *Nucl. Phys.* **B337**, 569 (1990).
- [2] E. Braaten and R. D. Pisarski, Resummation and Gauge Invariance of the Gluon Damping Rate in Hot QCD, *Phys. Rev. Lett.* **64**, 1338 (1990).
- [3] E. Braaten and R. D. Pisarski, Simple effective Lagrangian for hard thermal loops, *Phys. Rev. D* **45**, R1827 (1992).
- [4] J. O. Andersen, E. Braaten, and M. Strickland, Hard-Thermal-Loop Resummation of the Free Energy of a Hot Gluon Plasma, *Phys. Rev. Lett.* **83**, 2139 (1999).
- [5] J. O. Andersen, E. Braaten, E. Petitgirard, and M. Strickland, Hard-thermal-loop perturbation theory to two loops, *Phys. Rev. D* **66**, 085016 (2002).
- [6] P. Chakraborty, M. G. Mustafa, and M. H. Thoma, Quark number susceptibility in hard thermal loop approximation, *Eur. Phys. J. C* **23**, 591 (2002).
- [7] P. Chakraborty, M. G. Mustafa, and M. H. Thoma, Chiral susceptibility in the hard thermal loop approximation, *Phys. Rev. D* **67**, 114004 (2003).
- [8] P. Chakraborty, M. G. Mustafa, and M. H. Thoma, Quark-number susceptibility, thermodynamic sum rule, and the hard thermal loop approximation, *Phys. Rev. D* **68**, 085012 (2003).
- [9] J. O. Andersen, E. Petitgirard, and M. Strickland, Two-loop hard-thermal-loop thermodynamics with quarks, *Phys. Rev. D* **70**, 045001 (2004).
- [10] N. Su, J. O. Andersen, and M. Strickland, Gluon Thermodynamics at Intermediate Coupling, *Phys. Rev. Lett.* **104**, 122003 (2010).
- [11] J. O. Andersen, M. Strickland, and N. Su, Three-loop HTL gluon thermodynamics at intermediate coupling, *J. High Energy Phys.* **08** (2010) 113.
- [12] N. Haque and M. G. Mustafa, A modified hard thermal loop perturbation theory, [arXiv:1007.2076](https://arxiv.org/abs/1007.2076).
- [13] J. O. Andersen, L. E. Leganger, M. Strickland, and N. Su, NNLO hard-thermal-loop thermodynamics for QCD, *Phys. Lett. B* **696**, 468 (2011).
- [14] J. O. Andersen, L. E. Leganger, M. Strickland, and N. Su, Three-loop HTL QCD thermodynamics, *J. High Energy Phys.* **08** (2011) 053.
- [15] N. Haque, M. G. Mustafa, and M. H. Thoma, Conserved density fluctuation and temporal correlation function in hard thermal loop perturbation theory, *Phys. Rev. D* **84**, 054009 (2011).
- [16] J. O. Andersen, S. Mogliacci, N. Su, and A. Vuorinen, Quark number susceptibilities from resummed perturbation theory, *Phys. Rev. D* **87**, 074003 (2013).
- [17] N. Haque, M. G. Mustafa, and M. Strickland, Two-loop hard thermal loop pressure at finite temperature and chemical potential, *Phys. Rev. D* **87**, 105007 (2013).
- [18] S. Mogliacci, J. O. Andersen, M. Strickland, N. Su, and A. Vuorinen, Equation of state of hot and dense QCD: Resummed perturbation theory confronts lattice data, *J. High Energy Phys.* **12** (2013) 055.
- [19] N. Haque, M. G. Mustafa, and M. Strickland, Quark number susceptibilities from two-loop hard thermal loop perturbation theory, *J. High Energy Phys.* **07** (2013) 184.
- [20] N. Haque, J. O. Andersen, M. G. Mustafa, M. Strickland, and N. Su, Three-loop pressure and susceptibility at finite temperature and density from hard-thermal-loop perturbation theory, *Phys. Rev. D* **89**, 061701 (2014).
- [21] N. Haque, A. Bandyopadhyay, J. O. Andersen, M. G. Mustafa, M. Strickland, and N. Su, Three-loop HTLpt thermodynamics at finite temperature and chemical potential, *J. High Energy Phys.* **05** (2014) 027.
- [22] M. Strickland, J. O. Andersen, A. Bandyopadhyay, N. Haque, M. G. Mustafa, and N. Su, Three loop HTL perturbation theory at finite temperature and chemical potential, *Nucl. Phys.* **A931**, 841 (2014).
- [23] J. O. Andersen, N. Haque, M. G. Mustafa, M. Strickland, and N. Su, Equation of state for QCD at finite temperature and density. Resummation versus lattice data, *AIP Conf. Proc.* **1701**, 020003 (2016).
- [24] J. Kapusta, P. Lichard, and D. Seibert, High-energy photons from quark–gluon plasma versus hot hadronic gas, *Phys. Rev. D* **44**, 2774 (1991).
- [25] E. Braaten, R. D. Pisarski, and T.-C. Yuan, Production of Soft Dileptons in the Quark-Gluon Plasma, *Phys. Rev. Lett.* **64**, 2242 (1990).
- [26] C. Greiner, N. Haque, M. G. Mustafa, and M. H. Thoma, Low-mass dilepton rate from the deconfined phase, *Phys. Rev. C* **83**, 014908 (2011).
- [27] M. G. Mustafa, M. H. Thoma, and P. Chakraborty, Screening of a moving parton in the quark-gluon plasma, *Phys. Rev. C* **71**, 017901 (2005).
- [28] P. Chakraborty, M. G. Mustafa, and M. H. Thoma, Wakes in the quark-gluon plasma, *Phys. Rev. D* **74**, 094002 (2006).
- [29] M. H. Thoma, Damping rate of a hard photon in a relativistic plasma, *Phys. Rev. D* **51**, 862 (1995).
- [30] A. Abada and N. Daira-Aifa, Photon damping in one-loop HTL perturbation theory, *J. High Energy Phys.* **04** (2012) 071.
- [31] R. D. Pisarski, Damping rates for moving particles in hot QCD, *Phys. Rev. D* **47**, 5589 (1993).
- [32] S. Peigné, E. Pilon, and D. Schiff, The heavy fermion damping rate puzzle, *Z. Phys. C* **60**, 455 (1993).
- [33] E. Braaten and R. D. Pisarski, Calculation of the gluon damping rate in hot QCD, *Phys. Rev. D* **42**, 2156 (1990).
- [34] S. Mrowczynski and M. H. Thoma, Hard loop approach to anisotropic systems, *Phys. Rev. D* **62**, 036011 (2000).
- [35] P. Romatschke and M. Strickland, Collective modes of an anisotropic quark-gluon plasma, *Phys. Rev. D* **68**, 036004 (2003).
- [36] P. Romatschke and M. Strickland, Collective modes of an anisotropic quark-gluon plasma: II, *Phys. Rev. D* **70**, 116006 (2004).
- [37] E. Braaten and M. H. Thoma, Energy loss of a heavy fermion in a hot QED plasma, *Phys. Rev. D* **44**, 1298 (1991).
- [38] E. Braaten and M. H. Thoma, Energy loss of a heavy quark in the quark-gluon plasma, *Phys. Rev. D* **44**, R2625 (1991).
- [39] M. H. Thoma and M. Gyulassy, Quark damping and energy loss in the high temperature QCD, *Nucl. Phys.* **B351**, 491 (1991).
- [40] P. Romatschke and M. Strickland, Energy loss of a heavy fermion in an anisotropic QED plasma, *Phys. Rev. D* **69**, 065005 (2004).

- [41] P. Romatschke and M. Strickland, Collisional energy loss of a heavy quark in an anisotropic quark-gluon plasma, *Phys. Rev. D* **71**, 125008 (2005).
- [42] M. G. Mustafa, Energy loss of charm quarks in the quark-gluon plasma: Collisional vs radiative losses, *Phys. Rev. C* **72**, 014905 (2005).
- [43] C. P. Kießig and M. Plümacher, Hard-thermal-loop corrections in leptogenesis II: Solving the Boltzmann equations, *J. Cosmol. Astropart. Phys.* **09** (2012) 012.
- [44] C. P. Kießig and M. Plümacher, Hard-thermal-loop corrections in leptogenesis I: CP -asymmetries, *J. Cosmol. Astropart. Phys.* **07** (2012) 014.
- [45] P. Graf and F. D. Steffen, Thermal axion production in the primordial quark-gluon plasma, *Phys. Rev. D* **83**, 075011 (2011).
- [46] S. Nadkarni, Non-Abelian Debye screening. II. The singlet potential, *Phys. Rev. D* **34**, 3904 (1986).
- [47] P. Arnold and L. G. Yaffe, Non-Abelian Debye screening length beyond leading order, *Phys. Rev. D* **52**, 7208 (1995).
- [48] S. Borsányi, Z. Fodor, S. D. Katz, S. Krieg, C. Ratti, and K. Szabó, Fluctuations of conserved charges at finite temperature from lattice QCD, *J. High Energy Phys.* **01** (2012) 138.
- [49] S. Borsányi, G. Endrődi, Z. Fodor, S. D. Katz, S. Krieg, C. Ratti, and K. K. Szabó, QCD equation of state at nonzero chemical potential: Continuum results with physical quark masses at order μ^2 , *J. High Energy Phys.* **08** (2012) 053.
- [50] A. Bazavov *et al.*, Strangeness at High Temperatures: From Hadrons to Quarks, *Phys. Rev. Lett.* **111**, 082301 (2013).
- [51] A. Bazavov, H.-T. Ding, P. Hegde, F. Karsch, C. Miao, S. Mukherjee, P. Petreczky, C. Schmidt, and A. Velytsky, Quark number susceptibilities at high temperatures, *Phys. Rev. D* **88**, 094021 (2013).
- [52] C. Bernard, T. Burch, C. DeTar, J. Osborn, S. Gottlieb, E. B. Gregory, D. Toussaint, U. M. Heller, and R. Sugar (MILC Collaboration), QCD thermodynamics with three flavors of improved staggered quarks, *Phys. Rev. D* **71**, 034504 (2005).
- [53] A. Bazavov *et al.*, Equation of state and QCD transition at finite temperature, *Phys. Rev. D* **80**, 014504 (2009).
- [54] A. Bazavov *et al.* (HotQCD Collaboration), Fluctuations and correlations of net baryon number, electric charge, and strangeness: A comparison of lattice QCD results with the hadron resonance gas model, *Phys. Rev. D* **86**, 034509 (2012).
- [55] S. Datta, R. V. Gavai, and S. Gupta, PoS Lattice **2013**, 202 (2014).
- [56] H.-T. Ding, A. Francis, O. Kaczmarek, F. Karsch, E. Laermann, and W. Soeldner, Thermal dilepton rate and electrical conductivity: An analysis of vector current correlation functions in quenched lattice QCD, *Phys. Rev. D* **83**, 034504 (2011).
- [57] O. Kaczmarek and A. Francis, Electrical conductivity and thermal dilepton rate from quenched lattice QCD, *J. Phys. G* **38**, 124178 (2011).
- [58] G. Aarts and J. M. Martinez Resco, Transport coefficients, spectral functions and the lattice, *J. High Energy Phys.* **04** (2002) 053.
- [59] F. Karsch, E. Laermann, P. Petreczky, S. Stickan, and I. Wetzorke, A lattice calculation of thermal dilepton rates, *Phys. Lett. B* **530**, 147 (2002).
- [60] G. Aarts and J. M. Martinez Resco, Continuum and lattice meson spectral functions at nonzero momentum and high temperature, *Nucl. Phys.* **B726**, 93 (2005).
- [61] M. Asakawa, T. Hatsuda, and Y. Nakahara, Maximum entropy analysis of the spectral functions in lattice QCD, *Prog. Part. Nucl. Phys.* **46**, 459 (2001).
- [62] Y. Nakahara, M. Asakawa, and T. Hatsuda, Hadronic spectral functions in lattice QCD, *Phys. Rev. D* **60**, 091503 (1999).
- [63] I. Wetzorke and F. Karsch, in *Proceedings of the International Workshop on Strong and Electroweak Matter*, edited by C. P. Korthals-Altes (World Scientific, Singapore, 2001), p. 193.
- [64] A. Schäfer and M. H. Thoma, Quark propagation in a quark-gluon plasma with gluon condensate, *Phys. Lett. B* **451**, 195 (1999).
- [65] M. G. Mustafa, A. Schäfer, and M. H. Thoma, Gluon condensate and non-perturbative quark-photon vertex, *Phys. Lett. B* **472**, 402 (2000).
- [66] A. Peshier and M. H. Thoma, Quark Dispersion Relation and Dilepton Production in the Quark-Gluon Plasma, *Phys. Rev. Lett.* **84**, 841 (2000).
- [67] P. Chakraborty, M. G. Mustafa, and M. H. Thoma, Screening masses in gluonic plasma, *Phys. Rev. D* **85**, 056002 (2012).
- [68] P. Chakraborty and M. G. Mustafa, $D = 2$ gluon condensate and QCD propagators at finite temperature, *Phys. Lett. B* **711**, 390 (2012).
- [69] P. Chakraborty, Quasiquarks in melting gluon condensate, *J. High Energy Phys.* **03** (2013) 120.
- [70] G. Boyd, J. Engels, F. Karsch, E. Laermann, C. Legeland, M. Lütgemeier, and B. Petersson, Thermodynamics of SU(3) lattice gauge theory, *Nucl. Phys.* **B469**, 419 (1996).
- [71] M. G. Mustafa, A. Schäfer, and M. H. Thoma, Nonperturbative dilepton production from a quark-gluon plasma, *Phys. Rev. C* **61**, 024902 (1999); Gluon condensate, quark propagation, and dilepton production in the quark-gluon plasma, *Nucl. Phys.* **A661**, 653 (1999).
- [72] M. Kitazawa and F. Karsch, Spectral properties of quarks at finite temperature in lattice QCD, *Nucl. Phys.* **A830**, 223c (2009).
- [73] O. Kaczmarek, F. Karsch, M. Kitazawa, and W. Söldner, Thermal mass and dispersion relations of quarks in the deconfined phase of quenched QCD, *Phys. Rev. D* **86**, 036006 (2012).
- [74] T. Kim, M. Asakawa, and M. Kitazawa, Dilepton production spectrum above T_c with a lattice propagator, *Phys. Rev. D* **92**, 114014 (2015).
- [75] N. Su and K. Tywoniuk, Massless Mode and Positivity Violation in Hot QCD, *Phys. Rev. Lett.* **114**, 161601 (2015).
- [76] V. N. Gribov, Quantization of non-Abelian gauge theories, *Nucl. Phys.* **B139**, 1 (1978).
- [77] D. Zwanziger, Local and renormalizable action from the gribov horizon, *Nucl. Phys.* **B323**, 513 (1989).
- [78] A. Maas, Gauge bosons at zero and finite temperature, *Phys. Rep.* **524**, 203 (2013).

- [79] D. E. Kharzeev and E. M. Levin, Color Confinement and Screening in the θ Vacuum of QCD, *Phys. Rev. Lett.* **114**, 242001 (2015).
- [80] R. Jackiw, Coulomb gauge description of large Yang-Mills fields, *Phys. Rev. D* **17**, 1576 (1978).
- [81] D. Zwanziger, Equation of state of gluon plasma from local action, *Phys. Rev. D* **76**, 125014 (2007).
- [82] K. Fukushima and N. Su, Stabilizing perturbative Yang-Mills thermodynamics with Gribov quantization, *Phys. Rev. D* **88**, 076008 (2013).
- [83] J. A. Gracey, Two loop correction to the Gribov mass gap equation in Landau gauge QCD, *Phys. Lett. B* **632**, 282 (2006).
- [84] A. Bazavov, N. Brambilla, X. Garcia i Tormo, P. Petreczky, J. Soto, and A. Vairo, Determination of α_s from the QCD static energy, *Phys. Rev. D* **86**, 114031 (2012).
- [85] L. D. McLerran and T. Toimela, Photon and dilepton emission from the quark-gluon plasma: Some general considerations, *Phys. Rev. D* **31**, 545 (1985).
- [86] L. Van Hove, The Occurrence of Singularities in the Elastic Frequency Distribution of a Crystal, *Phys. Rev.* **89**, 1189 (1953).
- [87] N. W. Ashcroft and N. D. Mermin, *Solid State Physics* (Saunders College, Philadelphia, 1976).
- [88] J. Cleymans, J. Fingberg, and K. Redlich, Transverse-momentum distribution of dileptons in different scenarios for the QCD phase transition, *Phys. Rev. D* **35**, 2153 (1987).
- [89] D. Forster, *Hydrodynamics Fluctuation, Broken Symmetry and Correlation Function* (Benjamin/Cummings, Menlo Park, CA, 1975); H. B. Callen and T. A. Welton, Irreversibility and generalized noise, *Phys. Rev.* **83**, 34 (1951); R. Kubo, Statistical-mechanical theory of irreversible processes. I. General theory and simple applications to magnetic and conduction problems, *J. Phys. Soc. Jpn.* **12**, 570 (1957).
- [90] T. Kunihiro, Quark-number susceptibility and fluctuations in the vector channel at high temperatures, *Phys. Lett. B* **271**, 395 (1991).